

T. von Kalle  
M. Langendörfer  
F. F. Fernandez  
P. Winkler

## Combined dynamic contrast-enhancement and serial 3D-subtraction analysis in magnetic resonance imaging of osteoid osteomas

Received: 24 December 2008  
Revised: 22 March 2009  
Accepted: 4 April 2009  
Published online: 15 May 2009  
© European Society of Radiology 2009

T. von Kalle (✉) · P. Winkler  
Department of Paediatric Radiology,  
Klinikum Stuttgart Olgahospital,  
Bismarckstr. 8,  
70176 Stuttgart, Germany  
e-mail: t.vonkalle@klinikum-stuttgart.de  
Tel.: +49-711-27873301  
Fax: +49-711-27873409

M. Langendörfer · F. F. Fernandez  
Department of Paediatric Orthopaedics,  
Klinikum Stuttgart Olgahospital,  
Bismarckstr. 8,  
70176 Stuttgart, Germany

**Abstract** The purpose of this study was to retrospectively correlate the results of dynamic contrast-enhanced magnetic resonance imaging (MRI) with histological and clinical diagnoses in patients with osteoid osteomas. Fifty-four patients with the MR diagnosis of osteoid osteoma were studied. MRI (1.5 Tesla) consisted of thin-section STIR sequences, dynamic 3D T1 gradient echo sequences during application of contrast material, and high-resolution postcontrast T1 spin echo sequences with fat saturation (maximum voxel size  $0.6 \times 0.6 \times 3.0$  mm). Evaluation was focused on serial image subtraction during the early phase after contrast injection and on time-intensity curves. The surrounding edema was helpful in finding the nidus in each lesion. In 49 of 54 patients (90.7%), the diagnosis of osteoid osteoma was certain or highly

probable (sensitivity 1.0, positive predictive value 0.91). A total of 38 of 54 osteoid osteomas were histologically proven. Five MRI diagnoses were regarded as false positives. A similar proportion has been reported for computed tomography. Tailored high-resolution MR examinations with dynamic contrast enhancement can reliably diagnose osteoid osteomas and exactly localize the nidus without radiation exposure. We propose a stepwise approach with STIR sequences, dynamic contrast-enhanced scanning, and high-resolution postcontrast T1 spin echo sequences with fat saturation.

**Keywords** Osteoid osteoma · Magnetic resonance imaging (MRI) · Dynamic scanning · Contrast enhancement · Peritumoral edema · Radiation exposure

### Introduction

Osteoid osteoma accounts for approximately 12% of benign skeletal neoplasms [1]. It typically causes significant nocturnally exacerbating pain, which is mediated by prostaglandin E2 [2] and responds to nonsteroidal anti-inflammatory drugs in 75% of cases [1]. Complete surgical excision of the nidus is curative. As open surgery has been increasingly replaced by minimally invasive procedures and as the lesion may also be treated with prostaglandin E2 inhibitors, a histological confirmation is usually not obtained. Therefore, diagnosis depends entirely on radiological imaging [3–6].

Computed tomography (CT) is widely accepted as the imaging method of choice because of its high morphological accuracy and the option of guiding minimally invasive treatment procedures. However, given the typical patient age between 10 and 25 years, this technique is limited by its inherent radiation exposure [7]. High-resolution magnetic resonance imaging (MRI) has the diagnostic potential to provide morphological information about the nidus and also to show the surrounding edema and joint effusions [8–10]. Based on the high vascularization of the nidus, which has recently been histologically confirmed [2], MR imaging with dynamic scanning of contrast enhancement has already been shown to be as or more effective in

identifying osteoid osteomas [11] than thin-section non-enhanced CT [12].

To date, however, MRI has not been regarded as a real diagnostic alternative [13–15]. Two main reasons seem to account for this low acceptance. First, delineation of a small nidus requires MR imaging with high spatial resolution comparable to that of CT [8, 13, 14, 16]. Second, the typical vascular contrast enhancement of the nidus is not depicted by static routine postcontrast MR sequences [11, 12].

Since 1996 we have employed an MRI protocol that combines high-resolution sequences and dynamic contrast enhancement. We have thereby focused on serial subtraction analysis of 3D data sets and time-intensity curves obtained by dynamic scanning. To evaluate diagnostic reliability, we retrospectively correlated the results of this combined MRI protocol with histological diagnoses and clinical outcomes.

## Patients, materials, and methods

### Patients

We retrieved data of patients with the diagnosis of osteoid osteoma from the databases of our radiology department. Patients who had at least one MR examination at our institution from 1996 to April 2007 were included in the study. Written informed consent for the examination was given by all patients or their parents. Our local institutional review board does not require special consent for retrospective analysis of anonymized patient data. The majority of patients were referred for MR imaging through the department of pediatric orthopedics of our hospital where all patients underwent thorough medical history and physical examinations initially and at follow-up. Symp-

toms were described as typical of an osteoid osteoma if bone or joint pain occurred predominantly at night and could be relieved by nonsteroidal anti-inflammatory agents (prostaglandin E2 inhibitors).

### Histology

Pathological diagnoses were extracted from written reports in patient data files. Data files of two pathology departments, where histological evaluations of all specimens were performed, were searched for osteoid osteomas that may have been missed by our MR examinations.

### MR imaging techniques

All examinations were performed with 1.5 Tesla scanners: Magnetom Vision until August 2004 and Magnetom Avanto thereafter (both Siemens Healthcare Sector). Maximum duration of an examination was 45 min until 2004 and 30 min thereafter. During the examination children were accompanied by their parents. Patients were carefully positioned and immobilized by vacuum cushions to avoid movement artefacts. Flexible surface coils were invariably used.

Each examination started with thin-section STIR sequences in at least two orientations (Table 1). For dynamic scanning, we used a series of 13 3D T1 gradient echo (GE) sequences without fat saturation before August 2004 and with fat saturation thereafter. The 3D volume was designed to completely cover the affected bone region, marked by high signal intensity in STIR images, and enable both a sufficient temporal and spatial resolution to avoid missing a small nidus (Table 1). Each sequence lasted 30 s, resulting in 6.5 min duration of the whole dynamic MR

**Table 1** Imaging parameters

Sequence	Contrast material	TR (ms)	TE (ms)	TI (ms)	Slice thickness/ gap(mm)	FoV (mm)	Matrix	Voxel size (mm)	Duration/ k-space-center(min)
STIR 2D	Pre-contrast	5,300– 6,200	60	135	3–4/0.2–0.4	Tra 160–220× 160–220; cor, sag 180–300× 180–500	256×512	0.4–1.0×0.6– 1.5×3.0–4.0	2.5–5.5
T1 gradient echo 3D	Contrast- enhanced dynamic scanning	4.3	1.7	–	1.5–2.5/0	Tra, cor 160–210	256×256	0.6–0.8×0.6– 0.8×1.5–2.5	0.5/0.16
T1 spin echo 2D fat saturated	Post-contrast	400–630	11–20	–	2–3/0–0.3	Tra, cor, sag 160–210	256× 256–512	0.4–0.6×0.4– 0.6×2.0–3.0	2.5

*tra* Transverse plane, *cor* coronal, *sag* sagittal

data acquisition. Contrast material (0.2 ml/kg body weight, Magnevist, Bayer Schering Pharma) was manually injected within 1–2 s into a cubital vein between the first and second of 13 measurements, followed by 10–20 ml saline solution. Enhanced T1 spin echo (SE) sequences with fat suppression and high spatial resolution in one or two orientations were performed immediately after the dynamic MR acquisition.

### MRI data evaluation

Based on previous investigations, we defined a nidus as a clearly delineated round or oval intra-osseous lesion with smooth margins and a diameter below 1.6 cm [1]. Enhancement of the nidus was expected to be highest immediately after injection of contrast material. We use the term “nidus” for all lesions that meet these morphological criteria. Retrospective evaluation of all images and signal intensity data was performed by two experienced pediatric radiologists blinded to the histological findings and clinical outcome. The presence or absence of a nidus was assessed for STIR and contrast-enhanced T1 SE sequences. The number of slices that depicted the nidus, the presence of edema in the surrounding bone marrow and soft tissue as well as joint effusions and synovial thickening were recorded. In the case of interobserver disagreement, the decision was made in consensus meetings.

Data obtained during dynamic MR acquisition were analyzed in four steps at a commercially available workstation (Leonardo, Siemens Healthcare Sector)

1. Serial subtraction analysis: For each patient the data of the T1 GE sequence prior to contrast injection were subtracted from the data for each of the 12 postcontrast sequences [17]. The resulting 12 stacks of subtraction images were visually assessed. A round or oval intra-osseous enhancement in the early phase of dynamic scanning without apparent continuation into a blood vessel was identified as a possible nidus (Fig. 1a–c, e).
2. Time-intensity curves for the whole dynamic MR acquisition (6.5 min) were obtained for regions of interest (ROI) in the nidus (1 in Fig. 1c), in the adjacent tissue (bone marrow and soft tissue; 2 in Fig. 1c) and in small vessels outside the affected region (3 in Fig. 1c). These curves were compared in order to identify the point of the greatest difference between the signal intensities of the nidus and the adjacent tissue. The curve of the blood vessel served as control for adequate injection technique and as reference for a typical vascular pattern of enhancement [17].
3. To quantify the conspicuity of the nidus in the subtraction images, values of signal intensities were determined for the sequence with the greatest difference between nidus and adjacent tissue in the early phase of enhancement (*A* in Fig. 2), and for the last

sequence of the dynamic MR acquisition (late phase of enhancement; *B* in Fig. 2). For both sequences, the following ratio was calculated as described by Liu et al. [12]: signal intensity in the nidus/signal intensity in the adjacent tissue. A ratio below 1.0 would indicate a lower signal intensity in the nidus and a ratio above 1.0 a higher signal intensity in the nidus than in the adjacent tissue.

4. The nonsubtracted 3D data set with the greatest difference in signal intensities between nidus and adjacent tissue was reconstructed in multiple orientations to analyze the shape of the nidus and differentiate it from normal intra-osseous blood vessels (Fig. 3).

## Results

### Patients

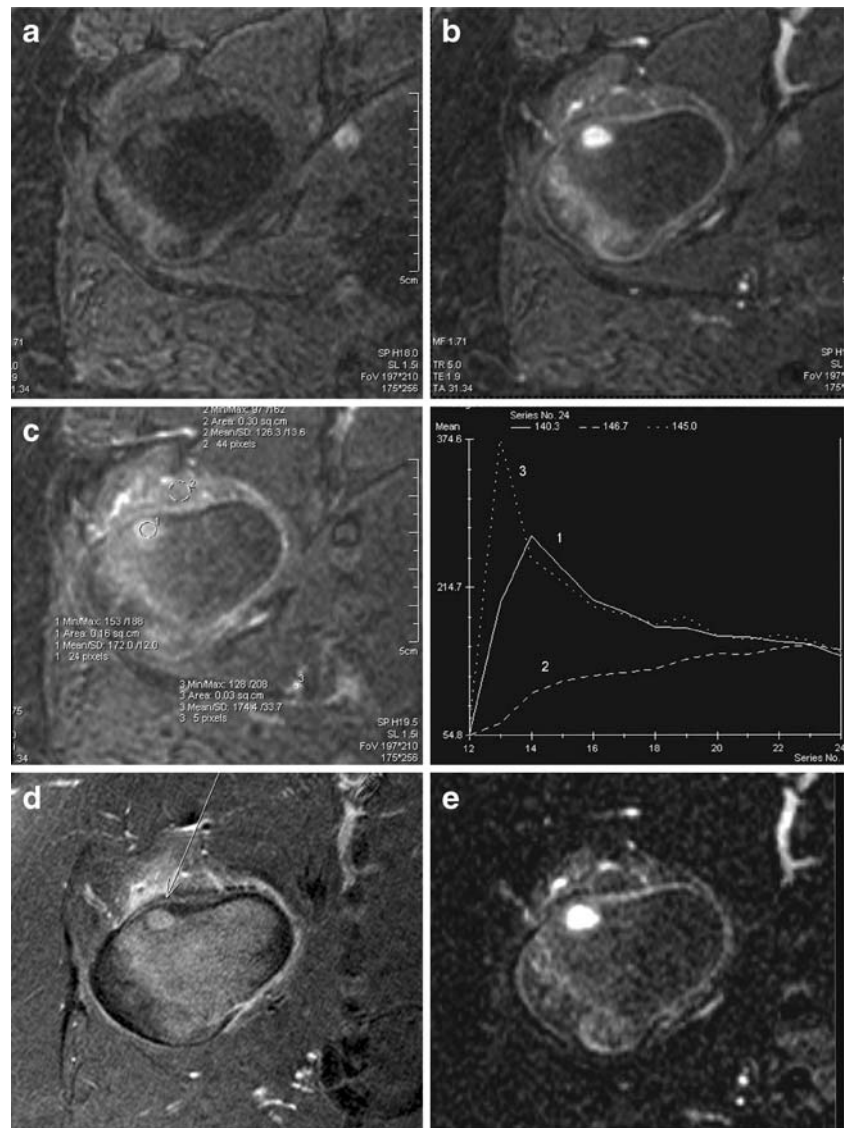
A total of 54 patients, 19 female and 35 male, with a median age of 10.3 years (1.4–38.8 years) were diagnosed by MRI and/or histology as having an osteoid osteoma and were included in our study. Three patients were older than 20 years, and five were younger than 5 years. Five of our youngest patients and one 9-year-old boy needed sedation for the diagnostic procedure. Nine lesions were removed by MR-guided minimally invasive procedures under general anesthesia. None of the examinations had to be aborted. No patient had to be referred for further diagnostic procedures except conventional radiographs, if these were not already available.

Before treatment, 34 of 54 patients (63%) had had clinical symptoms suggestive of osteoid osteoma. Complaints of 20 children (37%) were not typical.

Before being referred to our hospital, the diagnosis of osteoid osteoma had been highly probable in 10 of 54 patients, but localization of the nidus did not seem to be sufficient for the planning of surgery. In 44 patients, there had been no definite diagnosis, although all patients had had previous radiological examinations including radiographs in 44 patients, MRI in 35, CT in 8, scintigraphy in 9, and sonography in 3 patients. Eight patients had already undergone a biopsy. One of the 44 patients had gone through 11 diagnostic procedures including a biopsy. In 12 cases, osteoid osteoma was one of several differential diagnoses that included osteomyelitis (11 cases), meniscal tear, stress fracture, arthritis, Ewing’s sarcoma, chondrosarcoma, Legg-Calvé-Perthes disease, transient osteoporosis, soft-tissue lesion, and psychosomatic symptoms. None of our patients had had a dynamic contrast examination before being referred to our department.

Surgical treatment at our hospital consisted of en bloc resection, open drill excision or curettage and was the preferred method in most of the cases to allow a histological confirmation of the diagnosis. MRI-guided

**Fig. 1** Dynamic contrast-enhanced MRI. T1 GE images before (a), 1 min after (b), and 6 min after (c) contrast injection. c Time intensity curve of the nidus (1), the soft-tissue edema (2), and a blood vessel (3). X-axis presents time as the numbers of MR series, each lasting 30 s. Y-axis presents the mean signal intensity of the ROI (circles in c). Subtraction image (e) calculated from the data in images a and b. Excellent visibility of the nidus in the early phase of enhancement (b and e). Good visibility of the nidus in high-resolution postcontrast T1 SE with fat saturation (d)



intervention was performed by drill excision or laser ablation.

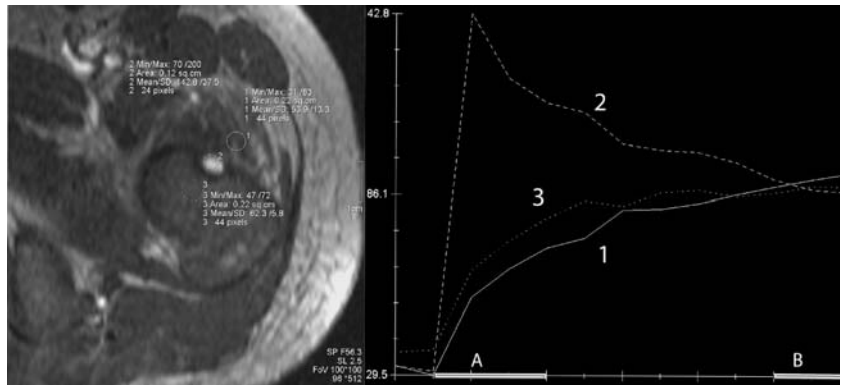
#### MRI: morphological results

A lesion that fulfilled the morphological and dynamic criteria for a nidus could be identified in the images of all 54 patients. Transverse diameter of the nidus ranged from 2 to 15 mm (median 6 mm), maximum diameter was below 2 cm. One nidus had a pin-shaped appearance with longitudinal length 1.8 cm and transverse diameter 0.5 mm. Most of the lesions were located in the lower extremities: femur  $n=28$ , tibia  $n=15$ , pedicles of the thoracolumbar spine  $n=5$ , calcaneus  $n=3$ , humerus  $n=2$ , and acetabulum  $n=1$ . Nearly all lesions were cortical or subcortical, only one was completely surrounded by bone

marrow. Three lesions were located subperiosteally, 14 were intra-articular, and none were in the epiphysis. STIR sequences showed a surrounding edema in all lesions and thus helped to focus the subsequent parts of the examination on the affected region. Signal intensity of the nidus in STIR images differed greatly between patients from high to medium to low intensities. Nidi with high intensities often had a low signal center. Each nidus could be identified in at least one slice of a STIR sequence (Fig. 4).

In high-resolution contrast-enhanced T1 SE sequences, performed after the dynamic MR acquisition, contrast enhancement of the nidus was not specific. However, a nidus could be delineated by morphological criteria in each lesion (Fig. 5). Depiction of structural details of the adjacent tissue allowed the exclusion of soft-tissue or bone-marrow tumors that might have been hidden in the high signal area of STIR images.

**Fig. 2** T1 GE image of the early phase of enhancement. Time-intensity curves of soft tissue (1), nidus (2), and bone marrow (3). Ratio between signal intensities of the nidus (2) and the surrounding tissue (1 and 3) is high in the early phase of enhancement (A) and low in the late phase (B)



### MRI: results of dynamic scanning

The maximum enhancement of each nidus occurred within the first 90 s after injection of contrast material. The time-intensity curves in 47 of 54 lesions had a characteristic shape that closely resembled that of small blood vessels: a steep rise at the beginning, a peak at the time of the first or second sequence after contrast injection (30–60 s) and a rapid continuous decrease in intensity (wash-out) thereafter (Figs. 1 and 2). Three confirmed osteoid osteomas showed a blunt or round peak at the second to third sequence, which was followed by a distinctive wash-out. Four lesions had a time-intensity curve with a rapid initial increase by the second postcontrast sequence, followed by a plateau or

a minimal wash-out (Fig. 6) (two histologically confirmed osteoid osteomas, one lesion without histology, and one classified as osteomyelitis).

Contrast kinetics in the adjacent tissue edema differed clearly from that of the nidus in all patients. Here the time-intensity curves increased gradually in the early phase after bolus injection, continuing to the end of measurement at 6.5 min or rising to a plateau (Figs. 1, 2 and 6).

Delineation of the nidus on subtraction or fat-suppressed images was best in the early phase (first 90 s) of contrast enhancement (Fig. 1b, e; A in Fig. 2). The median ratio of the signal intensities of the nidus and the adjacent tissue was 2.2 (range 1.0–6.7), which means that at the time of the peak in 30 of 54 nidi, the signal intensity was at least twice

**Fig. 3** Nidus (a, c) and vein (b, d) in the early phase of enhancement. Nidus (arrow in a) without continuation into adjacent blood vessels in 3D maximum intensity projection. Nidus (c) and blood vessel (d) not distinguishable in transverse 2D images

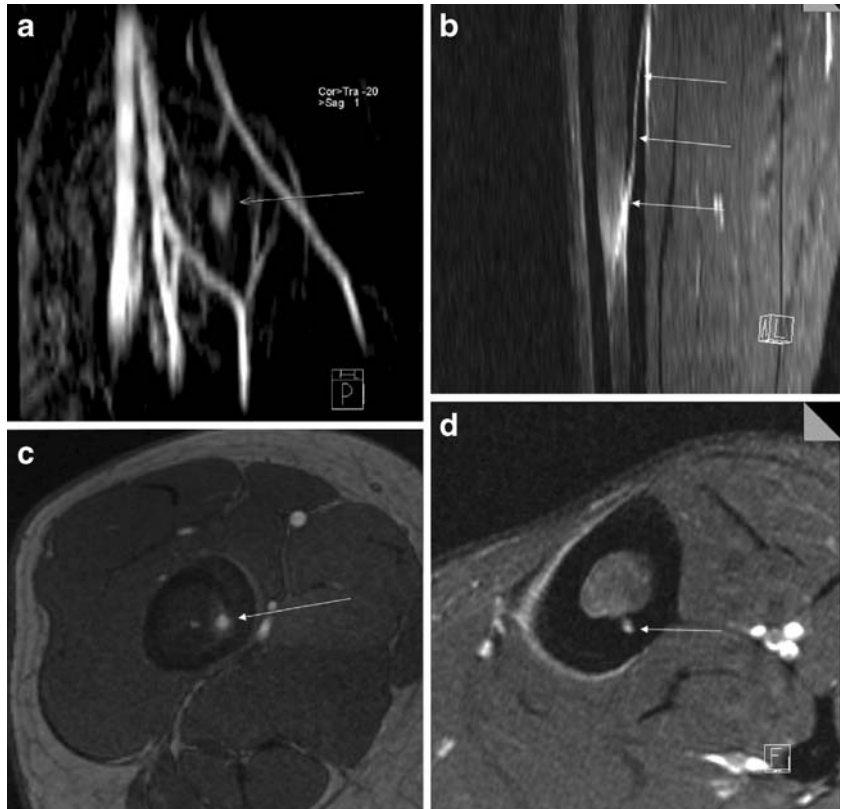
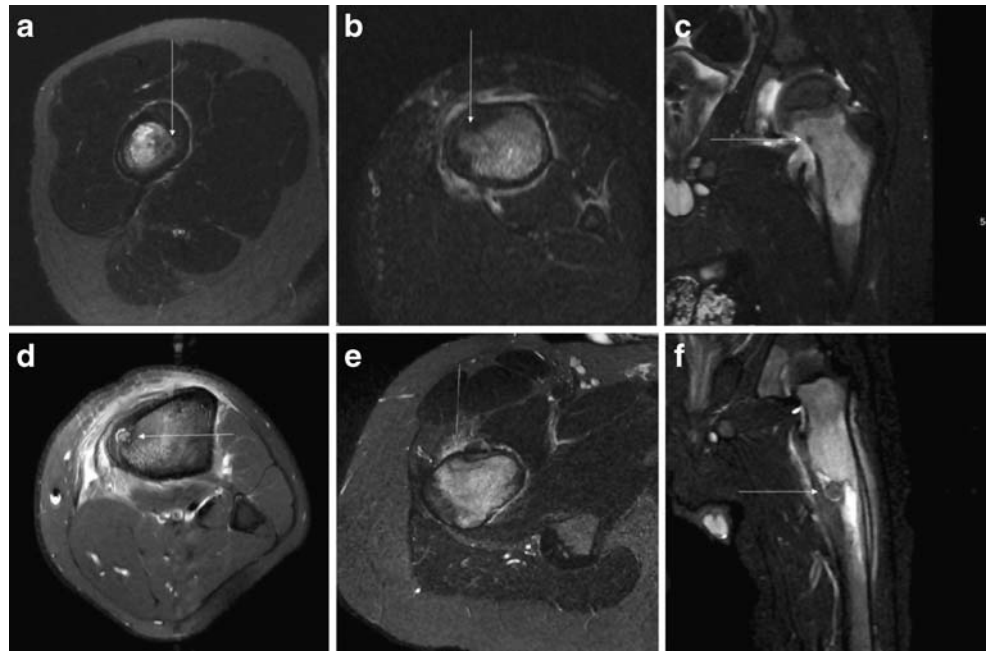


**Fig. 4** STIR images of six patients. Slice thickness 3–4 mm. Each nidus is clearly depicted (*arrows*) with variable signal intensities. Marked edema of the surrounding tissue helps to localize the nidus



as high as in the surrounding tissue. In one patient, both signal intensities were equal (ratio 1.0). This nidus could be clearly identified by its vascular time-intensity curve and the surrounding sclerosis. In the late phase, 6.5 min after contrast injection, the median ratio was 1.0 (range 0.4–4.0), which means that in 31 of 54 lesions, the signal intensity in the nidus either was equal to or below that of the adjacent structures. Therefore, in the late phase, a nidus could be identified only by morphological criteria and not by

differences in contrast (Fig. 5 and B in Fig. 2). Only in three lesions did the ratio remain above 2.

Multiplanar reconstruction of nonsubtracted T1 GE 3D data sets of the early phase allowed demonstration of the exact nidus localization in all its dimensions. Conspicuity in 3D or maximum-intensity projection (MIP) images was improved by fat suppression or subtraction of 3D data sets.

All time-intensity curves of blood vessels outside the perifocal edema showed a typical vascular enhancement

**Fig. 5** High-resolution post-contrast T1 SE images of six patients. Each nidus is clearly depicted by morphological criteria (*arrows*), but contrast enhancement is similar to that of the surrounding tissue

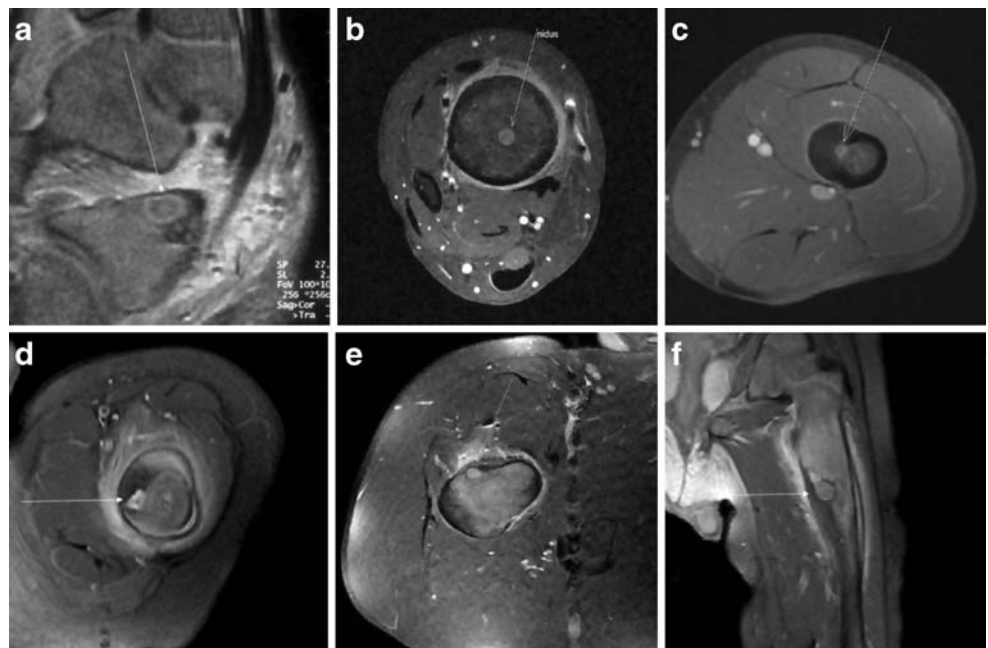
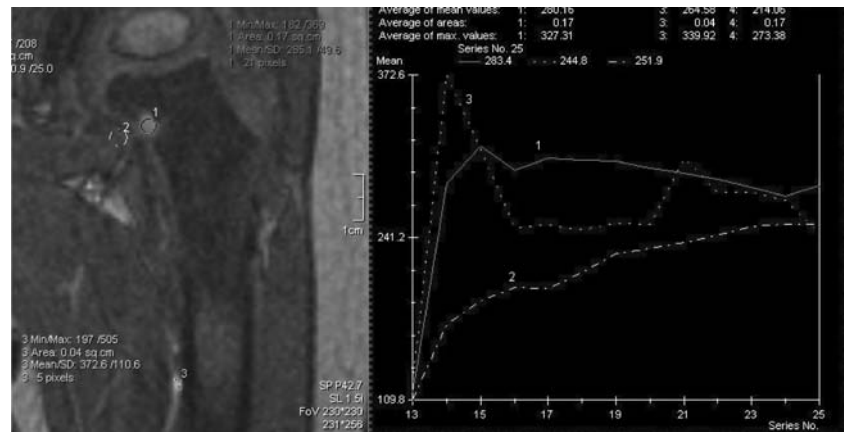


**Fig. 6** Patient with histologically confirmed osteoid osteoma. T1 GE image and time intensity: contrast enhancement in the nidus (1) with a rapid increase and a blunt peak followed by a slight decrease. Curves of adjacent soft tissue (2) and blood vessel (3)



with a peak followed by a wash-out (3 in Figs. 1 and 6). We therefore regard the manual bolus injection of contrast material to be adequate in all examinations. In our series, arteries and veins could be differentiated in 35 patients. A total of 27 lesions had a peak in the venous phase of enhancement and 8 in the arterial phase. With a temporal resolution of 30 s, a differentiation was not possible in 19 patients.

#### Correlation of MRI and histological results

Forty-eight specimens were available for histopathological analysis. A nidus was found in 38 of them (79% of 48 or 70% of all 54 patients) and thus confirmed the diagnosis of osteoid osteoma (Table 2). Three of these specimens

showed signs of chronic inflammation in the adjacent tissue.

In 10 specimens (18.5% of 54), there was no evidence of a nidus (Table 2). Histological findings in 2 of them were considered consistent with osteoid osteoma; a different histological diagnosis was assigned to 3 of the 10 specimens (Table 2). In the patient with nonossifying fibroma (NOF), MRI had shown two adjacent lesions, one compatible with NOF and the other with a nidus of an osteoid osteoma. The reports on the five remaining specimens described normal bone tissue, fibrosis, and/or sclerosis. In two of these patients, the nidus could still be depicted unchanged in situ by a postoperative MRI. The clinical course seemed consistent with osteoid osteoma in two patients, and with chronic osteomyelitis in one patient. Symptoms improved without further intervention. For six

**Table 2** Classification of patients according to histopathological results and clinical outcome

Diagnostic criteria	Number of patients			Probability of osteoid osteoma
	Nidus confirmed	Sample without nidus	No sample	
Osteoid osteoma confirmed by histology	38			Confirmed 38/54 (70%)
Histological findings consistent with osteoid osteoma		2		High 11/54 (20%)
Nidus still in situ on follow-up MRI		2		
No specific histological diagnosis, clinical course consistent with osteoid osteoma		2		
No tissue sample, clinical course consistent with osteoid osteoma			5	Low 5/54 (9%)
Specific histological diagnosis (osteomyelitis: $n=2$ , NOF: $n=1$ )		3		
No specific histological diagnosis, clinical course consistent with chronic osteomyelitis		1		
No tissue sample, clinical course consistent with CRMO			1	
Total number	38	10	6	54

NOF Nonossifying fibroma, CRMO chronic recurrent multifocal osteomyelitis

additional patients, tissue samples were not available (Table 2). In five of them, the clinical diagnosis was osteoid osteoma because of typical symptoms and clinical course.

In summary, 38 of 54 lesions were histologically confirmed osteoid osteomas, 11 lesions were not proven or not removed but followed a clinical course typical of osteoid osteoma, and 5 of 54 MRI diagnoses were regarded as false positives (Table 2). No false negative MR results were revealed. According to these data, the true positive rate or sensitivity to diagnose an osteoid osteoma was 1.0, and the positive predictive value was 0.91.

## Discussion

We chose a stepwise diagnostic approach (Table 3) with a combination of high spatial resolution and dynamic MRI. This combined technique proved to be helpful even in our series of 54 osteoid osteomas that were obviously difficult to diagnose, as can be inferred from the large proportion of inconclusive or erroneous prior examinations.

A total of 38 out of 54 MR diagnoses were confirmed by histology. To our knowledge, this is the largest series that has been published on proven osteoid osteomas diagnosed by MRI with dynamic contrast enhancement. We consider 11 of 54 lesions without histological confirmation to be osteoid osteomas because of the findings listed in Table 2. We therefore regard the MRI diagnosis of osteoid osteoma as certain or highly probable in 49 of 54 patients (90.7%) (Table 2).

If the histological results are considered as gold standard, 5 of our 54 MRI diagnoses (9.3%) have to be assumed to be false positive (Table 2). However, data of our study suggest that even specific histological diagnoses other than osteoid osteoma (three of these five patients, Table 2) do not completely rule out this diagnosis: in three cases of confirmed osteoid osteomas, tissue samples showed signs of inflammation near the nidus, and five

proven lesions had been diagnosed as osteomyelitis by earlier biopsies. As described above, the MR examination of the patient with histologically proven NOF had shown the osteoid osteoma adjacent to this second lesion.

The proportion of correct diagnoses of 90.7% in our study is comparable to the results reported for CT, which range from 3/5 (60%) patients [8], 14/21 (67%) [15], 26/32 (81%) [9], to 18/19 (94%) [14]. Studies on reliability of CT in the diagnosis of osteoid osteoma are rare despite long-term experience. Controlled trials are not available. Diagnosis by CT may be difficult in intra-articular and medullary osteoid osteomas [1, 8, 9]. Based on experiences with small numbers of histologically confirmed lesions, dynamic contrast-enhanced CT has been recommended to identify a nidus [16, 18, 19].

In each of our 54 patients, high signal intensity of bone marrow and soft tissue in STIR images correctly indicated the location of the nidus (Table 3). These findings are in line with other studies [8, 20–22, 24] and do not confirm reports on confounding MR results caused by the perifocal edema [14, 15, 23]. The superiority of nonenhanced MRI over CT in cases of noncortical osteoid osteomas has been claimed [8].

Each nidus could be differentiated morphologically in our high-resolution STIR (Fig. 4) and contrast-enhanced T1 SE images with fat saturation (Fig. 5). Studies that revealed high rates of false diagnoses of osteoid osteomas by MRI employed body coils and/or a magnetic field strength as low as 0.5 T [14] and relied on section thicknesses up to 10 mm [13] or in-plane resolution as low as  $1.6 \times 1.6$  mm [14], which resulted in low-resolution images [8, 13, 14] and low signal-to-noise ratios. Given a median nidus diameter of 6 mm in our series, it is obvious that small osteoid osteomas may be obscured by partial volume effects if in-plane resolution and section thickness are inadequate. In order to document the normal structures surrounding the nidus and thus exclude soft-tissue tumors, we consider high resolution and fat suppression (or subtraction analysis) essential in contrast-enhanced MRI.

**Table 3** Stepwise diagnostic approach in the MR diagnosis of osteoid osteoma

Step	Imaging technique	Imaging criterion
1. Region of interest	High-resolution STIR (or T2 fat suppressed) in one or two orientations	Region of interest marked by perifocal edema, nidus near the center with variable signal intensity
2. Identification of the nidus	Contrast-enhanced 3D dynamic T1 GE with adequate temporal and spatial resolution, covering the whole region of signal abnormality	Nidus visible in serial subtraction images of the first 30–90 s after injection
3. Signal intensity curve	Contrast-enhanced 3D dynamic T1 GE	Nidus with typical vascular shape of time-intensity curve
4. Morphology	Postcontrast T1 SE fat saturated, high resolution in at least one orientation	Morphological details of nidus, bone and soft tissue; exclusion of soft-tissue tumor
5. Differentiation from blood vessels	3D reconstruction T1 GE fat saturated in early phase, MIP	Round or oval shape of contrast-enhanced nidus, no continuation into blood vessels, no venous shape or branching



The importance of eliminating the fat signal has already been stressed in the MRI of neoplastic bone-marrow disorders [24].

In our series, the nidus could most reliably be traced and delineated with either subtraction or in fat-suppressed T1 GE images in the early phase of the dynamic contrast-enhanced MRI. The rapid initial increase in enhancement clearly separated the nidus from its surroundings in lesions with a sharp peak (47 of 54) (Fig. 1) as well as in those with a rounded peak or a plateau phase (7 of 54) (Fig. 6). These characteristic vascular enhancement patterns have been previously reported for single cases of osteoid osteomas examined with CT [6, 18, 19], MRI [17, 24, 25], scintigraphy [1], and angiography [1]. MRI studies focusing on enhancement kinetics of the nidus and its surroundings have been limited to small numbers of patients [11, 12]. In their study of 11 patients with histologically confirmed osteoid osteomas, Liu et al. [12] compared MR images with 6-mm section thickness and 1-mm gap to CT images of 2–3 mm with 50% section overlap. They concluded that, despite the lower spatial resolution, dynamic gadolinium-enhanced MR imaged osteoid osteomas with greater conspicuity than non-enhanced MRI and with a conspicuity equal to or better than thin-section CT.

The diffuse tissue enhancement without demarcation of the nidus in the late phase is explained by the gradual increase in contrast enhancement in tissue edema [24] that occurs simultaneously to its decrease (wash-out) in the nidus (Fig. 2). Static routine contrast-enhanced MR sequences are highly likely to miss the first 90 s after contrast injection. In combination with low spatial resolution, they have therefore been reported to be not appropriate for the depiction of a nidus [12, 14].

Differential diagnoses and potential pitfalls result from lesions that resemble a nidus either in its morphology or in its contrast kinetics. If assessed only in transverse sections, intra-osseous veins may easily be taken for a nidus. Meticulous search for continuation to larger vessels, which is facilitated by 3D data of the early phase of enhancement, helps to identify veins and to avoid this error (Fig. 3). Brodie's abscess may be morphologically indistinguishable from a nidus in MR [8] as well as in CT images [5, 6, 16, 18, 19]. In our experience, the contrast enhancement in chronic osteomyelitis increases more gradually than in osteoid osteomas and shows no clear-cut decrease (wash-out effect) in the late phase. This observation has been reported for CT [16, 19] and MRI [25] but has not yet been studied systematically. Other benign and malignant bone lesions may also show vascular patterns of enhancement [17, 24, 25], but in most cases they can be distinguished on MR imaging by different morphology, tumor site, and distribution of contrast enhancement [24]. Adequate bolus injection is a prerequisite for the correct interpretation of dynamic contrast enhancement. Manual injections should therefore

be cross-checked with time-intensity curves of small vessels, which should have a typical vascular enhancement pattern with a definite peak.

Fourteen osteoid osteomas of our series were located intra-articularly. Due to marked synovitis and bone-marrow edema, preceding clinical and radiological diagnoses typically were arthritis or Legg-Calvé-Perthes disease. This observation is in line with reports on intra-articular osteoid osteomas that were difficult to differentiate clinically and radiologically from other joint disorders [1, 9]. In these cases, in which findings on CT may be very subtle, multiplanar MR imaging [8] and, in our experience, dynamic contrast-enhanced MRI can be helpful. With these MRI techniques we also were able to differentiate between spinal osteoid osteoma and spondylolysis in a small number of patients.

The lack of direct and indirect radiation exposure is a great advantage of MRI over CT and an important issue for the typically young patient with osteoid osteoma (median age in our series 10.3 years). In 29 of our 54 cases, the nidus was in the proximal femur or the acetabulum, where radiation exposure of the reproductive organs is of particular concern in children and adolescents. Radiation exposure by CT might moreover increase considerably during dynamic scanning [18] and/or image-guided minimally invasive procedures and may thus contribute to the increasing medical radiation dose of children and adolescents, who have a high sensitivity and a long lifetime to develop radiation-induced cancer [7, 26]. A feasibility report on MRI-guided minimally invasive treatment of osteoid osteomas using a 0.23 T magnet has been published [27]. Our experience with a 1.5 T magnetic field is limited to nine interventions, all of which were successful and without complications.

There are limitations of our retrospective study. We cannot provide a systematic comparison of our findings to other imaging techniques or other bone lesions. As a result of evolving MR technology, our patients were examined with different MR techniques before and after 2004. As the vascular enhancement of osteoid osteomas has been documented by CT [16, 18, 19] as well as by different MRI devices [12], there is no evidence that this enhancement pattern depends on imaging techniques. Our data do not allow calculation of specificity and negative predictive value of the method. In case of inconclusive histological diagnosis, we had to rely on clinical outcome because in benign lesions relief of symptoms excluded repeated interventions. Prospective studies on sensitivity and specificity would most likely solve some of the questions raised by these limitations.

---

### Conclusions (implications for radiological practice)

From our series we conclude that tailored high-resolution MR examinations combined with dynamic contrast en-

hancement can reliably diagnose osteoid osteomas and exactly localize the nidus. We propose a systematic stepwise approach as listed in Table 3. The surrounding edema is helpful in finding the focus especially if the affected region cannot be identified on conventional radiographs or CT. Serial subtraction analysis (or fat-saturated T1 sequences) of the early phase after contrast injection and evaluation of time-intensity curves of enhancing lesions within the zone of edema are indis-

pensable. The overall duration of the examination is well tolerated by children, for whom the lack of radiation exposure is an important advantage over CT. MR-guided minimally invasive treatment seems to be feasible.

**Acknowledgements** The authors acknowledge Prof. Dr. K. Wurster, Munich, Dr. F. Prantl, Munich, and Dr. Wiedorn, Stuttgart, for their kind support.

## References

- Kransdorf MJ, Stull MA, Gilkey FW, Moser RP (1991) From the archives of the AFIP. Osteoid osteoma. Radiographics 11:671–696
- De Chadarévian JP, Katselos CD, Pascasio JM, Geller E, Herman MJ (2007) Histological study of osteoid osteoma's blood supply. *Pediatr Dev Pathol* 10:358–368
- Cantwell CP, Obyrne J, Eustace S (2004) Current trends in treatment of osteoid osteoma with an emphasis on radiofrequency ablation. *Eur Radiol* 14:607–617
- Ghanem I (2006) The management of osteoid osteoma: updates and controversies. *Curr Opin Pediatr* 18:36–41
- Vanderschueren GM, Taminiou AHM, Obermann WR, van den Berg-Huysmans AA, Bloem JL, van Erkel AR (2007) The healing pattern of osteoid osteomas on computed tomography and magnetic resonance imaging after thermocoagulation. *Skeletal Radiol* 36:813–821
- Woertler K, Vestring T, Boettner F, Winkelmann W, Heindel W, Lindner N (2001) Osteoid osteoma: CT-guided percutaneous radiofrequency ablation and follow-up in 47 patients. *J Vasc Interv Radiol* 12:717–722
- Goske MJ, Applegate KE, Boylan J, Butler PF, Callahan MJ, Coley BD, Farley S, Frush DP, Hernanz-Schulman M, Jaramillo D, Johnson ND, Kaste SC, Morrison G, Strauss KJ, Tuggle N (2008) The 'image gently' campaign: increasing CT radiation dose awareness through a national education and an awareness program. *Pediatr Radiol* 38:265–269
- Spouge AR, Thain LMF (2000) Osteoid osteoma: MR imaging revisited. *J Clin Imaging* 24:19–27
- Szendroi M, Koello K, Antal I, Lakatos J, Szoke G (2004) Intraarticular osteoid osteoma: clinical features, imaging results, and comparison with extraarticular localization. *J Rheumatol* 31:957–964
- Kayser F, Resnick D, Haghighi P, Do Rosario Husch Pereira E, Greenway G, Schweitzer M, Kindynis P (1998) Evidence of the subperiosteal origin of osteoid osteoma in tubular bones: analysis by CT and MR imaging. *AJR* 170:609–614
- Von Kalle T, Winkler P, Walz P, Wolf R, Wurster K (2001) Is MRI helpful in hidden cases of osteoid osteoma? The significance of dynamic scanning. *Pediatr Radiol* 31:S15
- Liu PT, Chivers FS, Roberts CC, Schultz CJ, Beauchamp CP (2003) Imaging of osteoid osteoma with gadolinium-enhanced MR imaging. *Radiology* 227:691–700
- Davies M, Cassar-Pullicino VN, Davies AM, McCall IW, Tyrrell PNM (2002) The diagnostic accuracy of MR imaging in osteoid osteoma. *Skelet Radiol* 31:559–569
- Assoun J, Richardi G, Railhac JJ, Baunin C, Fajadet P, Giron J, Maquin P, Haddad J, Bonneville P (1994) Osteoid osteoma: MR imaging versus CT. *Radiology* 191:217–223
- Hosalkar HS, Garg S, Moroz L, Pollock A, Dormans JP (2005) The diagnostic accuracy of MRI versus CT imaging for osteoid osteoma in children. *Clin Orthop Relat Res* 433:171–177
- Woertler K (2003) Benign bone tumors and tumor-like lesions: value of cross-sectional imaging. *Eur Radiol* 13:1820–1835
- Van der Woude HJ, Verstraete KL, Hogendoorn PCW, Taminiou AHM, Hermans J, Bloem JL (1998) Musculoskeletal tumors: does fast dynamic contrast-enhanced subtraction MR imaging contribute to the characterization? *Radiology* 208:821–828
- Levine E, Neff JR (1983) Dynamic computed tomography scanning of benign bone lesions: preliminary results. *Skelet Radiol* 9:238–245
- McGrath BE, Bush CH, Nelson TE, Scarborough MT (1996) Evaluation of suspected osteoid osteoma. *Clin Orthop Relat Res* 327:247–252
- Nogués P, Martí-Bonmatí L, Aparisi F, Saborido MC, Garci J, Dosdá R (1998) MR imaging assessment of juxta cortical edema in osteoid osteoma in 28 patients. *Eur Radiol* 8:236–238
- Ehara S, Rosenthal DI, Aoki J, Fukuda K, Sugimoto H, Mizutani H, Okada K, Hatori M, Abe M (1999) Peritumoral edema in osteoid osteoma on magnetic resonance imaging. *Skelet Radiol* 28:265–270
- Woods ER, Martel W, Mandell SH, Crabbe JP (1993) Reactive soft-tissue mass associated with osteoid osteoma: correlation with pathologic findings. *Radiology* 186:221–225
- Alyas F, James SL, Davies AM, Saifuddin A (2007) The role of MR imaging in the diagnostic characterization of appendicular bone tumours and tumour-like conditions. *Eur Radiol* 17:2675–2686
- Van der Woude HJ, Egmont-Petersen M (2001) Contrast-enhanced magnetic resonance imaging of bone marrow. *Sem Musculoskelet Radiol* 5:21–33
- Verstraete KL, Dierckx A, De Deene Y, Uyttendaele D, Vandamme F, Roels H, Kunnen M (1994) First-pass images of musculoskeletal lesions: a new and useful diagnostic application of dynamic contrast-enhanced MRI. *Magn Reson Imaging* 12:687–702
- Brenner DJ, Hall EJ (2007) Computed tomography - an increasing source of radiation exposure. *N Engl J Med* 357:2277–2284
- Blanco Sequeiros R, Hyvönen P, Blanco Sequeiros A, Jyrkinen L, Ojala R, Klemola R, Vaara T, Tervonen O (2003) MR imaging-guided laser ablation of osteoid osteomas with use of optical instrument guidance at 0.23 T. *Eur Radiol* 13:2309–2314